Preferred citation: G. Bellani, F. Lundell and L.D. Söderberg. Experimental study of filtration of fiber suspensions: Part I: time-resolved measurements of the formation of a fiber network. In **Advances in Pulp and Paper Research, Oxford 2017**, *Trans. of the XVIth Fund. Res. Symp. Oxford, 2017*, (W. Batchelor and D. Söderberg, eds), pp 255–280, FRC, Manchester, 2018. DOI: 10.15376/frc.2017.1.255.

EXPERIMENTAL STUDY OF FILTRATION OF FIBER SUSPENSIONS

PART I: TIME-RESOLVED MEASUREMENTS OF THE FORMATION OF A FIBER NETWORK

Gabriele Bellani[1], *Fredrik Lundell*[1] *and L. Daniel Söderberg*[1,2]

[1] Linné Flow Centre, KTH Mechanics, SE-100 44 Stockholm, Sweden
[2] Innventia AB, SE-114 86 Stockholm, Sweden

ABSTRACT

We present a new laboratory apparatus designed to study the filtration of a fiber suspension in a parameter range close to that of the real papermaking process. An experimental procedure that combines index-of-refracion matching, high-speed imaging, and Particle Image Velocimetry (PIV) is used to measure flow and particle dynamics. In particular we presents results for: flow above a mesh similar to that used for paper forming; flow above and in the forming fiber network; evolution of the structure of the fiber network itself. Experiments are performed varying filtration velocity and fiber length. The results show that flow perturbations in the proximity of the mesh and the forming network are confined in a thin region and the height of this region are likely to scale with the pore size. Snapshots of the flow in the formed fiber network are also presented. These snapshot reveal qualitative differences between the networks formed by fibers of different lengths.

1 INTRODUCTION

Fibrous porous media are important in many technological applications, such as production of composite materials [13], [17], [14], gas cleaners [6], papermaking [7]. In many these applications the porous media is formed due to the filtration of a fiber suspension through a filter medium (such as, for example a perforated plate or a woven wire).

An example is the initial dewatering phase in papermaking, which is the main focus of this study. During initial dewatering, a fiber suspension with mass concentration of about $\phi < 0.5\%$ is filtered through a screen (referred to as *forming wire* or *fabric*). Here the fibers start to form the paper sheet and at the end of this process more than 20% of the water is removed. At this concentrations, fiber mobility is greatly reduced, hence this process has a large impact on the final structure of the paper sheet. Many investigations studied the impact of initial dewatering on paper structure. In the 1960s it was suggested that high dewatering rates have an "healing" effect on fiber distribution on a paper sheet, and this effect was quantified experimentally by [9]. The explanation is that if a hole is present in the web during the dewatering phase, the local dewatering resistance will be low resulting in an increased flow that transports more fibers and thereby heals the hole.

Also the geometry of the forming fabric is of great importance for the de-watering capacity. [1] studied the effects of wire design on sheet properties in laboratory forming. [5] points out that fabric surface aperture size has to be chosen with consideration of the fiber length distribution if dewatering capacity has to be optimized. [16] designed a closed water flow loop in which the desired amount of fibers can be injected and a web collected on an inserted fabric, at dewatering rates similar to those during initial forming. The results showed that the fabric structure has a big influence on the surface layer of the paper, showing a high correlation between fabric openings and fiber location, during the early stages of dewatering.

These studies reported macroscopic effects of the main parameters involved in the dewatering process. However, the physical mechanisms behind the macroscopic effects is to be sought in the hydrodynamic interactions between fiber and fluid phase occurring during filtration (the impact of fluid mechanics in papermaking is discussed in detail in [10]). These interactions can be explained as follows: (i) the structure of the filtered cake affecting the incoming flow (*e.g.* pressure drop is intrinsically connected to the microstructure of the fiber network, see for example refs. [21], [18]), and (ii) the incoming flow affecting network structure. For example [23] have shown that fiber entanglement (hence mechanical strength of the network) is coupled to fluid vorticity.

Studying the whole filtration process experimentally is challenging because it involves multi-scale two-phase flow measurements with particle phase often

blocking optical access to the fluid phase. [19] and [2] used index of refraction matching techniques to measure the flow in the proximity and inside a porous medium, but in their measurements the structure of the porous media was kept constant, so that the flow was stationary. Instead, in the filtration process the fiber network is constantly evolving, thus non-stationarity of the flow has to be taken into account. Simulations are a promising tool since they provide access to all quantities for both phases, but to perform a full-simulation of the filtration flow is computationally very expensive due to the strong coupling. Nevertheless, increasing computational power and improvements in numerical modeling make it possible to perform simulations of fiber flows in somewhat realistic parameter ranges [20], [11]. These tools will be extremely useful in the future, and they will replace to a large extent complex experimental investigations. However, numerical simulations cannot yet explore parameter ranges close to those encountered in the real applications, and, most importantly, they still need accurate description of physical mechanisms like fiber-fiber/fiber-wall interactions. Thus, highly resolved experiments are still greatly needed.

1.1 Present work

The aim of this work is to obtain an accurate and complete time-resolved description of the filtration process. In particular, we are interested in quantitative and qualitative information of the non-stationary flow generated during filtration in a parameter range close to the initial dewatering of the papermaking process, both above and in the fiber network. We are also interested in tracking the evolution of the structure of the fiber network in time. To achieve this this, we designed a scaled up laboratory apparatus where the filtration of a fiber suspension can be performed in a controlled and repeatable environment and an experimental procedure that combines index-of-refracion matching, high-speed imaging, and Particle Image Velocimetry (PIV).

1.2 Structure of the paper

The paper is structured as follows: we start with the description of the experimental setup and measurement techniques 2. In section 2.1 we present measurements of the flow through a forming fabric. In section 4 we present results of six experimental cases where we varied filtration velocity and fiber length. The results include quantitative analysis and statistics of the flow in the proximity of the growing fiber network and snapshots of the flow through the fiber network. Finally, in section 5 we discussed and summarize the results, both in light of fluid mechanics and of papermaking.

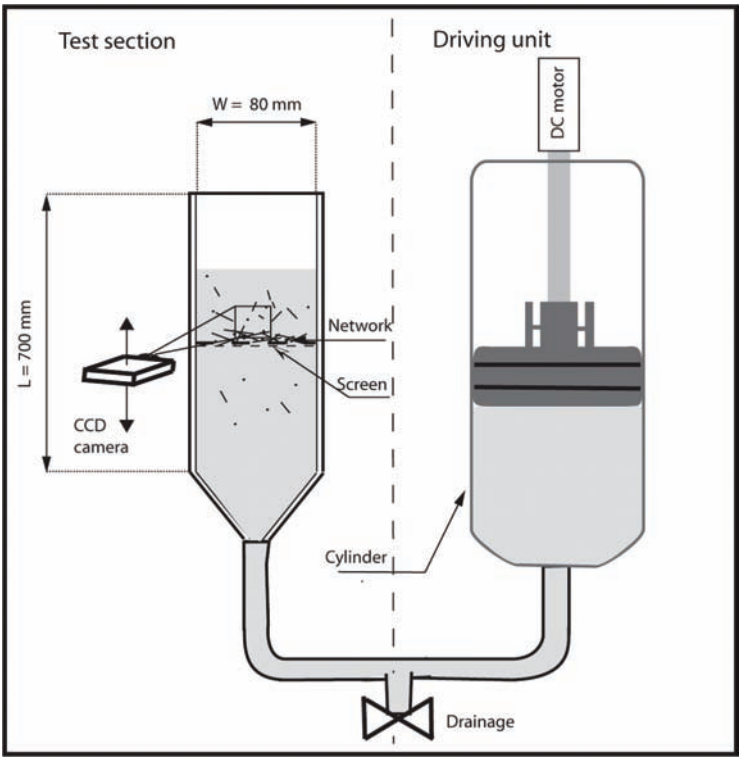

Figure 1. Experimental setup.

2 EXPERIMENTAL SETUP

The experimental apparatus consists of a test section and a driving unit (see Figure 1). The test section is a vertical transparent channel, filled with a fiber suspension, with a square cross-section of dimensions 80 × 80mm. At half of the channel length, a woven mesh is horizontally mounted across the section, where the fiber network can be formed.

The driving unit consists of a cylinder directly connected to the test section, and a piston. The piston is driven by a DC motor and controls the flow velocity by displacing the fluid in the system.

2.1 Characterization of the flow in the setup

In order to quantify the influence of the wall we need to check the extension of the boundary layer in the test section, and verify that there is a region where the

Table 1. Setup verification: experimental cases

	Case 1	*Case 2*	*Case 3*
Average velocity [mm/s]	V_m=21.5	V_m = 46.5	V_m = 96.4
Reynolds number	Re_D = 1565	Re_D = 3378	Re_D = 7011

incoming is uniform. Thus we perform a set of experiment aimed at characterizing the flow in the near wall region. Each experiment (realization) consists of two parts. In the first part we fill the test section until the free surface level reaches $Y^* = -100$ mm. In the second part the flow is driven down until the surface is at $Y^* = -40$ mm. No fibers are suspended in the flow. Images of the flow are captured during the second part, where the fluid flows through the screen (forming wire). In this section, the physical coordinates (X^*, Y^*) are scaled with the width of the test section D = 80 mm and the non-dimensional coordinates are:

$$X = \frac{X^*}{D} \qquad Y = \frac{Y^*}{D}. \tag{1}$$

Three realizations at different flow rates are performed. We will refer to the three realizations as Case 1, Case 2 and Case 3. The test was done keeping the flow rate constant during the entire realization, except from a short, transient acceleration at the start up. The corresponding average drainage velocity (V_m) for each realization is shown in Table 1. In the same table, the values of the Reynolds number Re_D based on the channel width D = 80 mm are also shown.

To get an idea of the shape of the velocity profiles in the test section as a function of Re_D we calculate the probability density function of the time resolved velocity measurements at $Y = -0.13$ for every point in X. The contours of the probability density functions of $v(X, Y, t)$ so obtained for Case 1, Case 2 and Case 3 are shown in Figure 2. It is clear that for every realization, there is a region where v is constant towards the center of the channel. In particular, the velocity seems to be unaffected by the boundary layer for $X > 0.2$.

2.2 Fibers and Index-of-Refraction matching

In order to have optical access through the fiber suspension, and thus be able to measure the flow in the fiber network, the index of refraction of fibers and fluid have been matched. The match is achieved using model fibers made of fluoropolymers (Tetrafluoroethylene, TFE) and a 65% solution of glycerin in water as suspending fluid. Fibers are available in two batches with different aspect ratios, r_p = 35 and r_p = 70. The dimensions and physical properties of fibers and fluid are

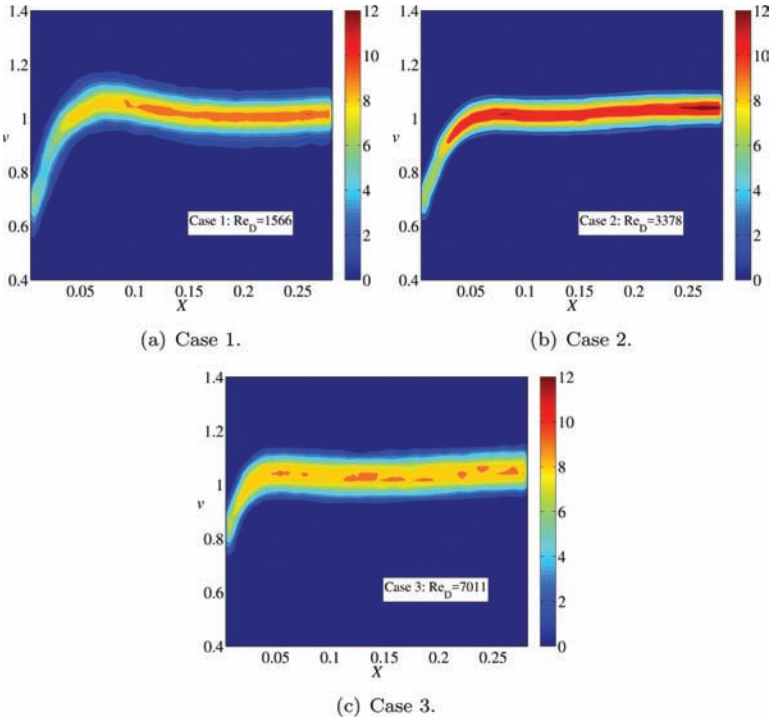

Figure 2. Probability density functions of v for Case 1 (a), Case 2 (b) and Case 3 (c).

shown in Table 2. In order to achieve measurements with a spatial resolution of the order of a fiber diameter, fibers and mesh size are about 10 times larger as compared to the papermaking case. However, since fluid viscosity is *circa* 15 times larger than water, the dynamic similarity, as measured by the Reynolds number based on fiber diameter and filtration velocity is preserved.

2.3 Measurement techniques

The measurement area is imaged at 200 fps with a CCD camera of resolution 640 × 480 pixels. The fluid phase is traced by polyamid seeding particles of diameter 20 μm. A 450 W cold light source is used to generate a light sheet of about 1 mm. A typical image is shown in Figure 3(a).

Thanks to Index-of-Refraction (IoR) matching, tracer particles moving through the fiber network are still visible. This allows us, through digital image processing, to decouple images of the tracers which mark the fluid phase, from the fibers, and analyze data separately. The digital filter used to process the images is described

Table 2. Summary of physical and geometrical properties of fluid, fibers and screen

Fluid properties	
density	$\varrho_f = 1.17$ g/cm^3
viscosity	$\mu_f = 1.52 \cdot 10^{-3}$ Pa · s
Fiber properties	
density	$\varrho_p = 1.8$ g/cm^3
length	$l_p = 9.4, 18.8$ mm
diameter	$d_p = 0.26$ mm
Screen	
wire diameter	$d_s = 1$ mm
grid spacing	$S = 2$ mm

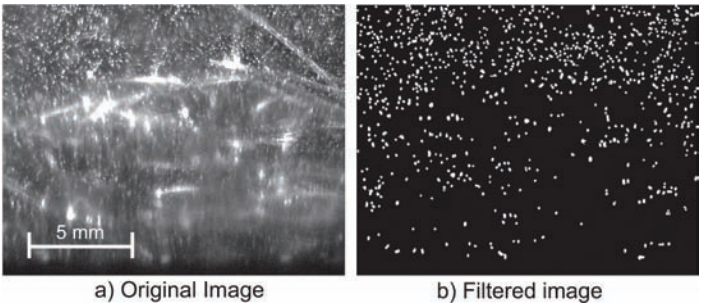

Figure 3. To the left, a typical snapshot of the filtration flow (a). Fluid tracers appear as small white dots, while fibers, still partly visible after the IoR matching are still partly visible. To the right, the outcome of digital image processing, where the fiber network have been removed and only tracer particles are visible.

in [4]. The outcome of the filtering procedure is shown in figure 3. From the images containing only the tracers is then possible to calculate the velocity field of the fluid phase by Particle Image Velocimetry (PIV) [22]. At the same time, we can use raw the images to track the evolution of the fiber network.

3 FLOW THROUGH THE FORMING WIRE

As discussed in the introduction, there is a strong, influence of the forming wire on the characteristics of the final sheet [16], [1], [5]. It is therefore interesting to analyze in detail the characteristics of the flow to a typical forming wire. Measurements are performed at $X > 0.2$, and therefore the velocity profiles are not affected

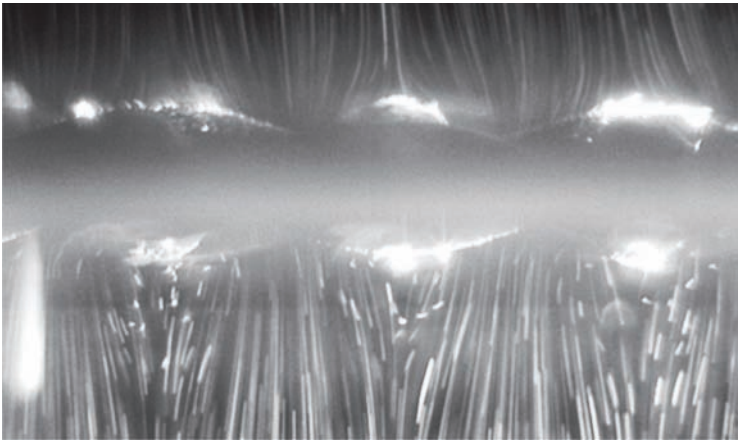

Figure 4. Streamlines above and below the forming fabric.

by the side walls (see section 2.1). The flow above the empty wire can be seen as the flow field generated by the filtration at $t = 0$, which determines the distribution of mass and orientation of the first layer of fibers in the network.

We run three experimental cases with increasing filtration velocity. The three cases are the seam as those described in section 2.1). Figure 4 show the the mean of 400 images acquired during one experimental case (Case 3), thus the lines marked by the tracer particles can be interpreted as the streamlines of the flow through (and below) the forming fabric. It can be seen that the streamlines get more dense in correspondence to the apertures in the fabric, as the flow as to accelerate to due to the reduce area. Therefore we can expect large velocity gradients in this area. In the next section we analyze the average velocity fields computed by PIV, and quantify the extent of these gradients.

3.1 Average velocity field

The mean velocity field $\bar{v}_t\,(x, y)$ for all the cases are shown in Figure 5(a, c, e). In this figure we also show the normalized velocity profiles at four positions corresponding to $y = -11.8, -8.1, 4.4, -0.7$. Here the coordinates are scaled with the wire diameter of the screen $d_s = 1$mm and the non-dimensional coordinates are:

$$x = \frac{X^* - X_C^*}{d_s} \qquad y = \frac{Y^*}{d_s}. \tag{2}$$

where $X_C^* = 25$ mm is the center of the region under study. The velocity profiles start to deform as we get close to the screen but they appear quite unaffected by

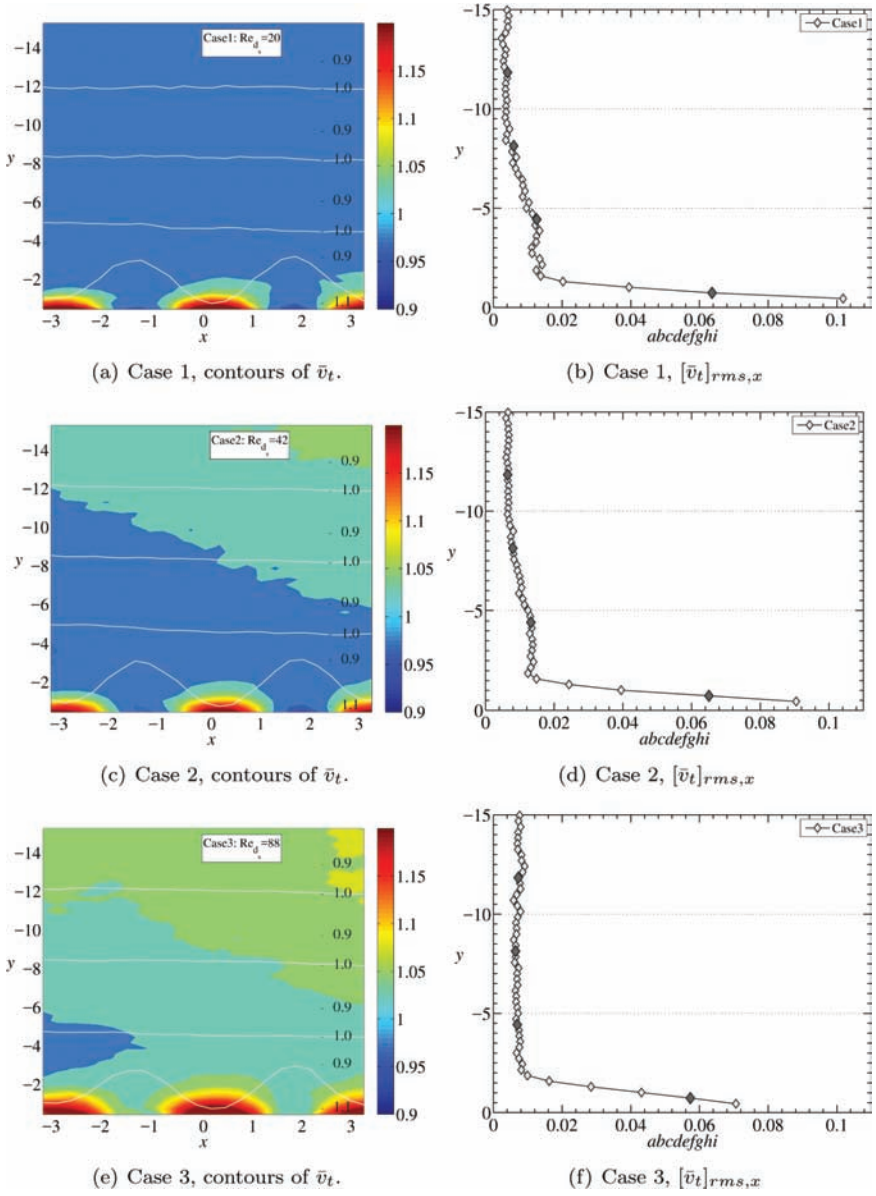

Figure 5. Contours of $\bar{v}_t$ ((a, c, e) and screen normal profiles of $[\bar{v}_t]_{rms,x}$ (b, d, f) for Case 1 (a, b), Case 2 (c, d) and Case 3 (d, f). The white lines in (a, c, e) show the normalized velocity profiles at $y = -11.8, -8.1, -4.4$ and -0.7.

the screen further out. One way to quantify where and how much the velocity profiles start to deform, thus creating spatial velocity gradients, is to analyze the *rms* of $\bar{v}_t$ in the horizontal direction, i.e. $[\bar{v}_t]_{rms,x}(y)$, which are shown in Figure 5(b, d, f). Significant deformation occurs only for $y > -2$.

It is also interesting to compare the screen-normal profiles of $[\bar{v}_t]_{rms,x}$ and study the influence of Re_{ds} on the level at which velocity fluctuations start to increase when approaching the screen. To do this, $[\bar{v}_t]_{rms,x}$ and $[\bar{u}_t]_{rms,x}$ are scaled with their respective maximum value and the results are shown in Figure 6. It appears that the shape of the rms profiles is independent of the Re_{ds}.

3.2 Boundary region

Figure 6 shows that flow perturbations introduced by the forming wire are confined in a thin region.

This result is of interest because in regions where the velocity field is uniform, no relative motion between the fibers is possible. In fact, changes in the distribution of mass and orientation of the fibers due to hydrodynamic effects are only possible in regions where the velocity gradients are non zero. No velocity gradients in the flow also mean zero vorticity, thus fiber entanglement is not promoted outside the region affected by the wire [23]. Although this analysis does not expose how the suspension microstructure is modified, it provides an estimation of the length scale over which the boundary can interact with the suspension. Here the height of the boundary region y_b can be defined as the level at which the 85% of the total "energy" ($E_{(f)}$) of a given quantity f is confined. Thus $y_b(_f)$ is defined so that:

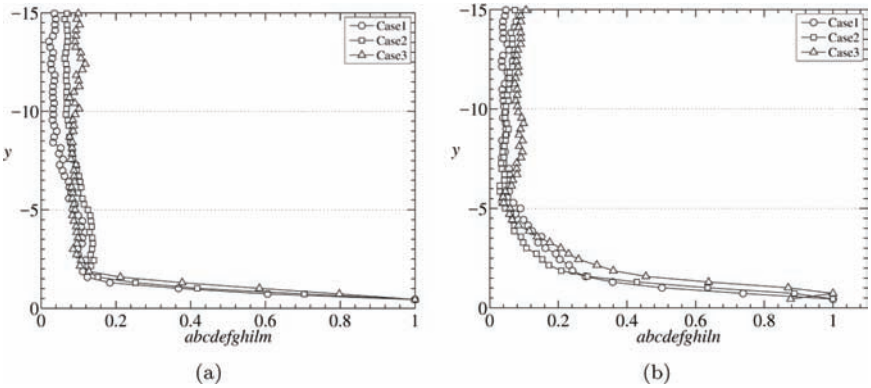

Figure 6. Normalized screen-normal profiles of (a) $[\bar{v}_t]_{rms,x}$ and (b) $[\bar{u}_t]_{rms,x}$ for Case 1, Case 2 and Case 3.

$$\frac{\int_0^{-y_{b(f)}} f(y)^2\, dy}{E_{(f)}} = 0.85 \tag{3}$$

$$E_{(f)} = \int_0^{-y_{max}} f(y)^2\, dy \tag{4}$$

where y_{max} is the total height of the image. From figure 6 we see that $-5 < y_b < -1$ for all quantities in the flow above the empty screen. The numerical values of the measured y_b are summarized in Table 3.

Table 3. Summary of y_b measurements

	Case 1	*Case 2*	*Case 3*
$y_b([\bar{v}_t]_{rms,x})$	–1.87	–3.72	–4.50
$y_b([\bar{v}_t]_{rms,x})$	–1.87	–1.30	–2.15

4 FILTRATION PROCESS

In this section we present results of measurement done during the filtration of a fiber suspension. The results comes from from six different cases, with all combinations of 3 different filtration velocities V_m, constant during each realization, and 2 fiber aspect ratios r_p. For each case we performed three realizations. The cases are denoted Case A, Case B, Case C, Case D, Case E and Case F, whereas the three realizations will be denoted by the progressive numbers 1, 2 and 3.

The values of fiber length l_p, filtration velocity V_m, Stokes velocity v_s (settling velocity assuming Stokes flow) and Stokes time $t_s = d_p/ v_s$, for each case are presented in Table 4. Table 5 contains the values of the non-dimensional parameters r_p, Re_{ds}, Re_{dp} and *Se*.

Table 4. Physical parameters of the experimental cases in section 4.3

Filtration velocity [mm/s]:		
$V_m = 20.5$	Case A	Case B
$V_m = 55.0$	Case C	Case D
$V_m = 75.2$	Case E	Case F
Fiber length [mm]:	l_p=18.8	l_p=9.4
Stokes velocity [mm/s]:	$v_s = 1.4$	$v_s = 1.2$
Stokes time $t_s = \frac{d_P}{v_s}$ [s]:	t_s=0.19	t_s=0.22

Table 5. Non-dimensional parameters

	Case A	*Case C*	*Case E*
$r_p = \frac{l_p}{d_p}$	r_p=72	r_p=72	r_p=72
$\mathrm{Re}_{d_m} = \frac{\rho_f V_m d_m}{\mu}$	Re_{dm} = 1.64	Re_{dm} = 4.4	Re_{dm} = 6
$\mathrm{Re}_{d_p} = \frac{\rho_f V_m d_p}{\mu}$	Re_{dp} = 0.43	$Re_{d}p$ = 1.14	Re_{dp} = 1.56
$Se = \frac{v_s}{V_m}$	*Se*=0.068	*Se*=0.026	*Se*=0.019
	Case B	*Case D*	*Case F*
$r_p = \frac{l_p}{d_p}$	r_p=36	r_p=36	r_p=36
$\mathrm{Re}_{d_m} = \frac{\rho_f V_m d_m}{\mu}$	Re_{dm} = 1.64	Re_{dm} = 4.4	Re_{dm} = 6
$\mathrm{Re}_{d_p} = \frac{\rho_f V_m d_p}{\mu}$	Re_{dp} = 0.43	Re_{dp} = 1.14	Re_{dp} = 1.56
$Se = \frac{v_s}{V_m}$	*Se*=0.059	*Se*=0.022	*Se*=0.016

4.1 Experimental procedure

The initial volume concentration of the suspension is about $\phi = 0.5 \cdot 10^{-2}$ for all the experiments. The concentration measure $N = \phi r_p^2$ is $N = 26$ for the suspension with the long fibers and $N = 6.5$ for the suspension with the short fibers. In both cases N is in the semi-dilute range [15].

Each realization consists of filling the test section until the suspension reaches $Y^* = -150$ mm, gently stirring the suspension with a propeller until a homogeneous distribution is obtained. The filtration phase begins at the end of the stirring, where the suspension is filtered through the screen until the free surface has reached $Y^* = -40$ mm. The suspension is seeded with tracer particles and images of the flow are captured during the filtration phase.

Figure 7 shows a typical image sequence of the filtration process: initially there is the (steady) flow through the empty mesh (as discussed in section 3), then the firs layers of fibers come and the network starts to build up forming a time-

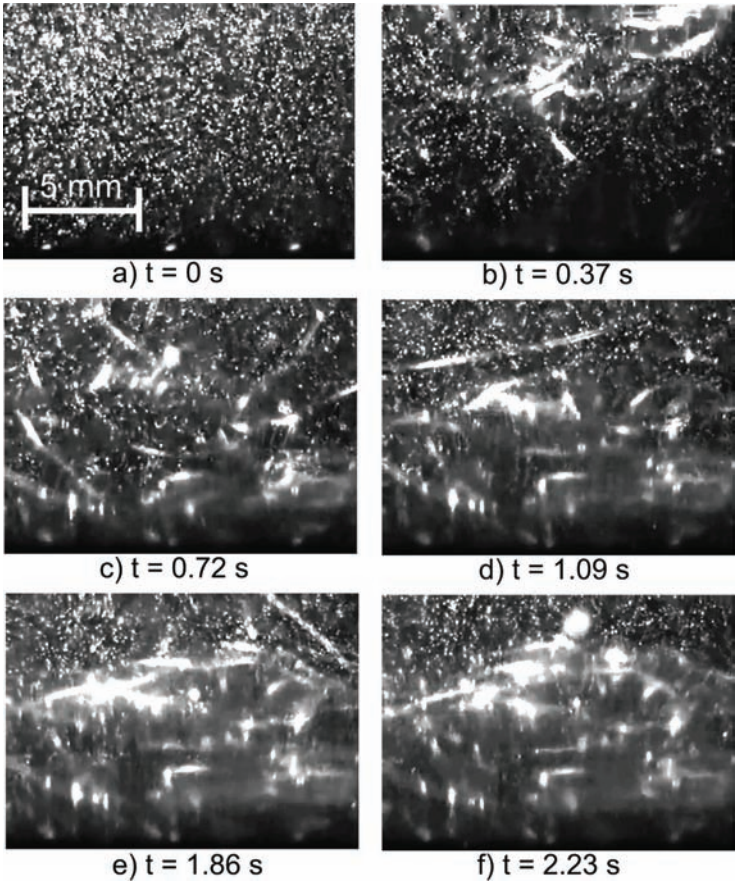

Figure 7. Experimental setup.

dependent boundary, and creating large and small scale velocity fluctuations. Finally when all the fibers have deposited on the network we have again a steady flow through the formed network.

The position of the measurement plane is shown in Figure 9. The center of the image window is located at $X = 0.35$.

4.2 Fiber accumulation

The time evolution of the average fiber network level h_f is extracted from the raw images analyzing the average grayscale values. This method exploit the fact that

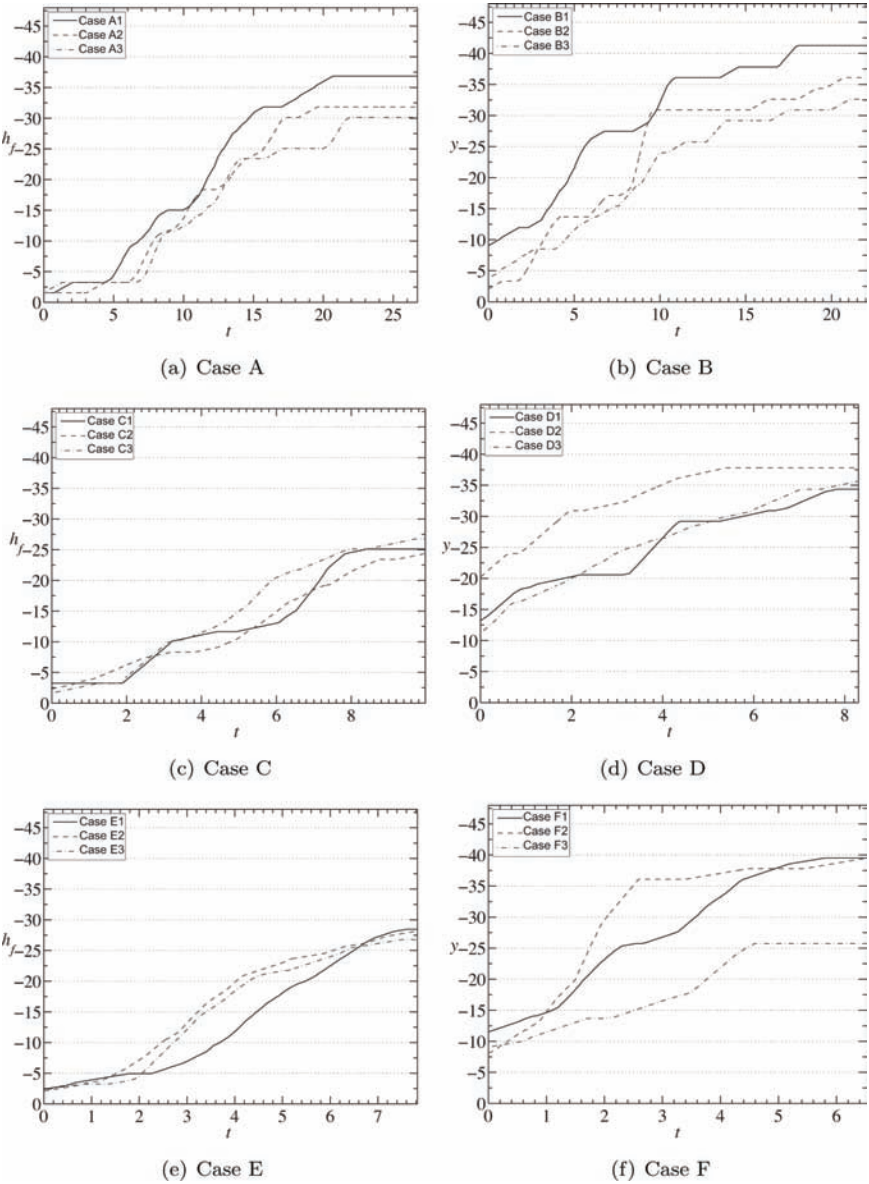

Figure 8. Evolution of the average height h_f of the fiber network, calculated from the analysis of the grayscale of the images.

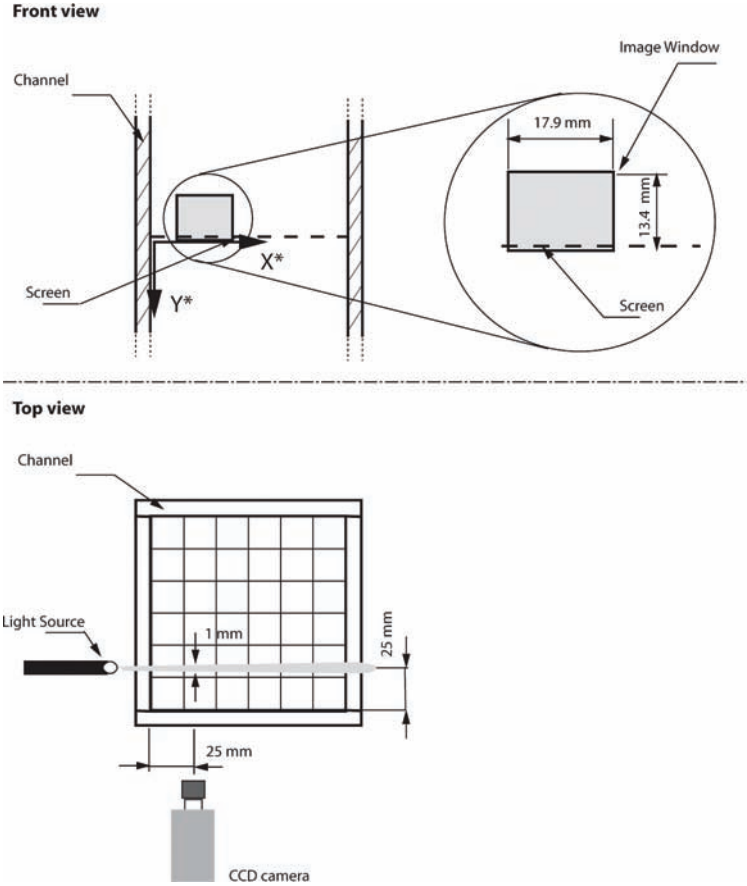

Figure 9. Position of the image window with respect to the coordinate system (X^*, Y^*) for the measurements presented in section 4.3. The camera is centered at $X^*_C = 25$ mm. In the close up the physical size of the image window (17.9 × 13.9 mm^2) is shown.

the regions with high fiber density have an average brightness higher than regions with only seeding particles. The resulting network level for all realizations are shown in Figure 8.

Observe that, a part from a small offset in initial/final network height due to fiber loss through the screen between consecutive realizations, the time-history of network height is similar between the three realization of the same case, showing a good consistency of the experimental procedure. The only exception is Case F, where the final network level is considerably lower for the third realization. This

is probably due to the fact that a larger portion of the fibers have been lost through the screen due to the combination of high filtration speed and short fibers.

4.3 Flow above the forming network

In this section we present measurements of the velocity field generated by the filtration of a fiber suspension in the direct proximity of the forming fiber network. The coordinates are here scaled with the fiber diameter d_p = 0.26 mm so that

$$x = \frac{X^* - X_C^*}{d_s} \qquad y = \frac{Y^*}{d_s}. \tag{5}$$

where X_C^* is the center of the region under study, in this case $X_C^* = 25$ mm.

Four snapshots of the instantaneous velocity v for Case A1 at different times are shown in Figure 10. The average level h_f of the fiber network is shown by the dark area in the figures. As anticipated, the figure shows that the flow structures are non-stationary, hence the flow quantities has to be analyzed as a function of time. In (a), there is an acceleration in a narrow region close to the screen. As the network grows, larger flow structures appear in (b), (c) and (d).

In order to quantify the deformation of the velocity profiles, in section 3 we investigated the horizontal rms of the average velocity field. In a similar fashion, here we calculate $v_{rms,x}$ for the instantaneous velocity fields.

Therefore, while in section 3 $[\bar{v}_t]_{rms,x}$ and $[\bar{u}_t]_{rms,x}$ were functions of y only, in this case, $v_{rms,x}$ and $u_{rms,x}$ are functions of time as well.

First, $v_{rms,x}$ is calculated for the three realizations of each case. The final $v_{rms,x}$ for one case is obtained as the average over the three realizations. Figure 11 shows the contours of $v_{rms,x}$ in the (y, t) plane, for all the cases. The average profile of the forming network is shown by the darker region. From these plots we can see that regions of high activity in the proximity of the network can be observed for the fast long fibre cases, Case C and Case E, whereas the correlation is less distinct for Case A, Case B, Case D and Case F. Although not shown here, the same behavior is observed for $u_{rms,x}$.

4.4 Boundary region

As in section 3.2, the height of a boundary region can be defined as

$$\frac{\int_0^{-yb(f)(t)} f(y,t)^2\, dy}{E(f)(t)} = 0.85 \tag{6}$$

$$E_{(f)}(t) = \int_0^{-y\max} f(y,t)^2\, dy. \tag{7}$$

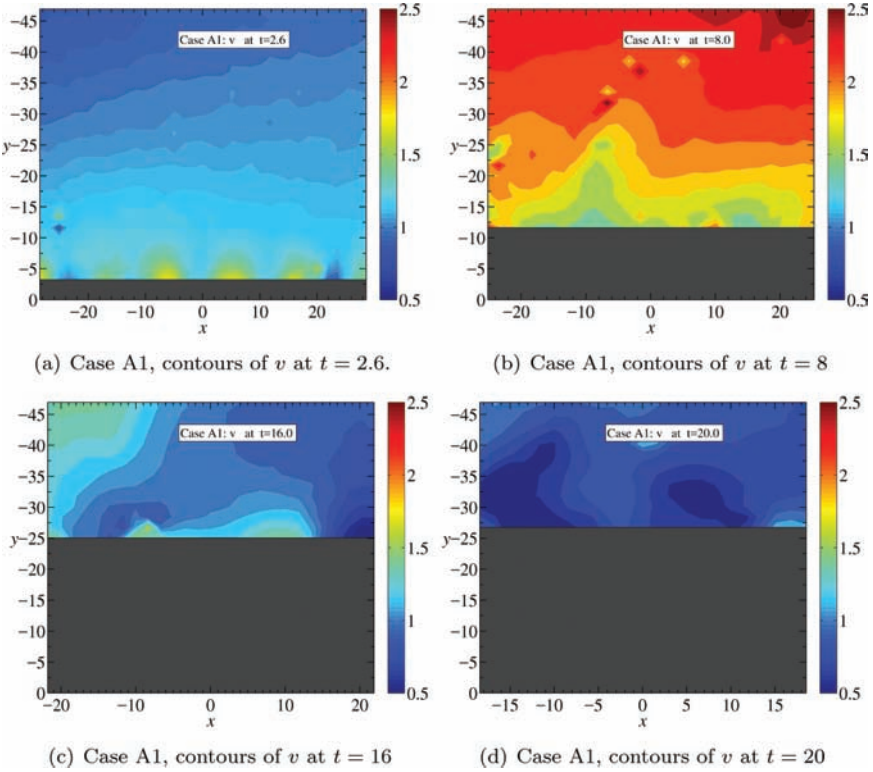

(a) Case A1, contours of v at $t = 2.6$. (b) Case A1, contours of v at $t = 8$

(c) Case A1, contours of v at $t = 16$ (d) Case A1, contours of v at $t = 20$

Figure 10. Contours of v for Case A1, at t = 2.6, 8.0, 16.0 and 20.0. The dark area is the average level of the fiber network, calculated from the analysis of the digital images.

Note that y_b and E are functions of time. Moreover, since the height of the boundary is also changing in time, the relevant measure becomes $y_b - h_f$.

The thickness of the boundary region has been calculated with $f = v_{rms,x}$ and $f = u_{rms,x}$; the results are shown in Figure 12. The results show that $y_b - h_f$ is time dependent. In most of the cases, at $t = 0$ we have $-20 < (y_b - h_f) < -15$. However, the general trend is that $y_b - h_f$ first increases with time as the network is formed, reaches a maximum, and then saturates at a fairly steady value. The final value is $(y_b - h_f) \approx 10$ for the cases with long fibers, but it is slightly lower for the cases with short fibers.

The same trend is observed for E_f (Figure 13), where the energy of the fluctuations reaches a maximum and then goes back to the initial value for the cases with short fibers, and to a value slightly higher for the cases with long fibers.

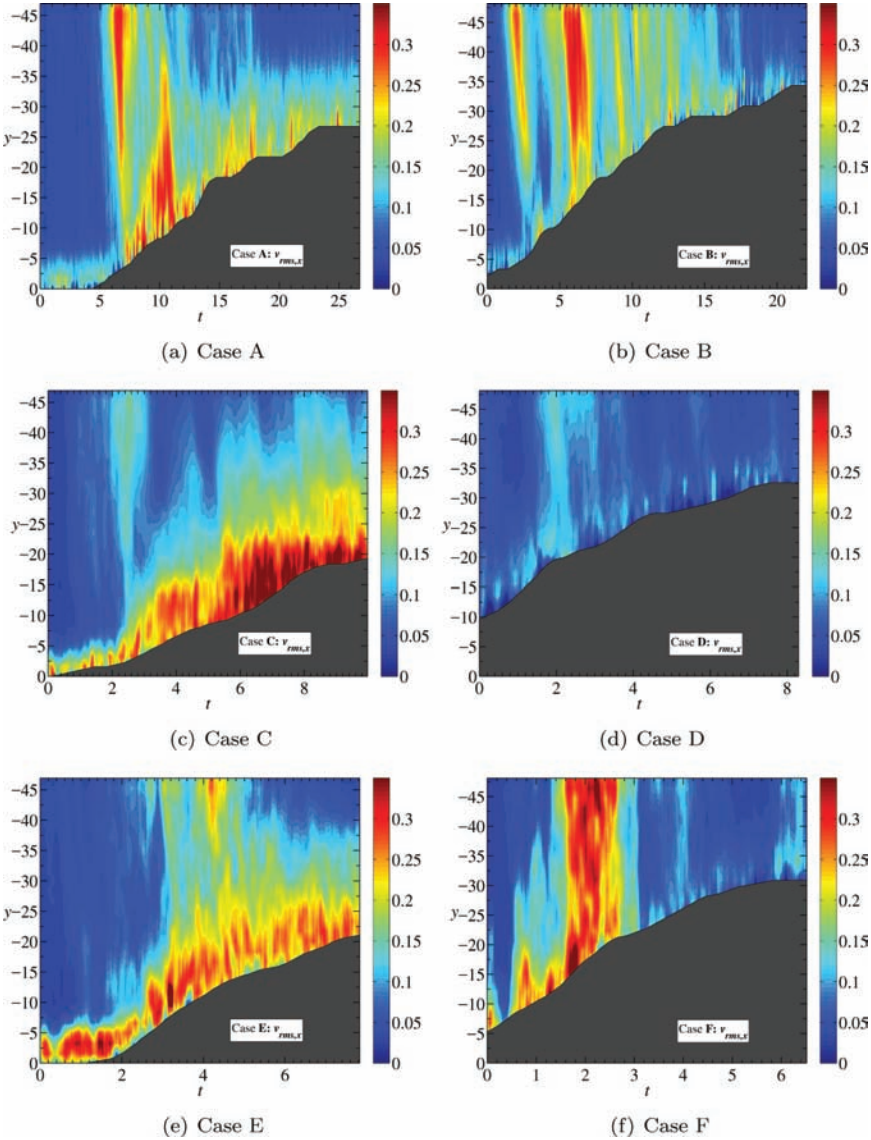

Figure 11. Contours of $v_{rms,x}$ as a function t/t_s and y/d_f for all cases. The values are normalized with the corresponding V_m. The dark area at the bottom right of each figure shows the evolution of the average height of the fiber network, h_f. In this figure, $v_{rms,x}$ is obtained from the average of 3 realizations.

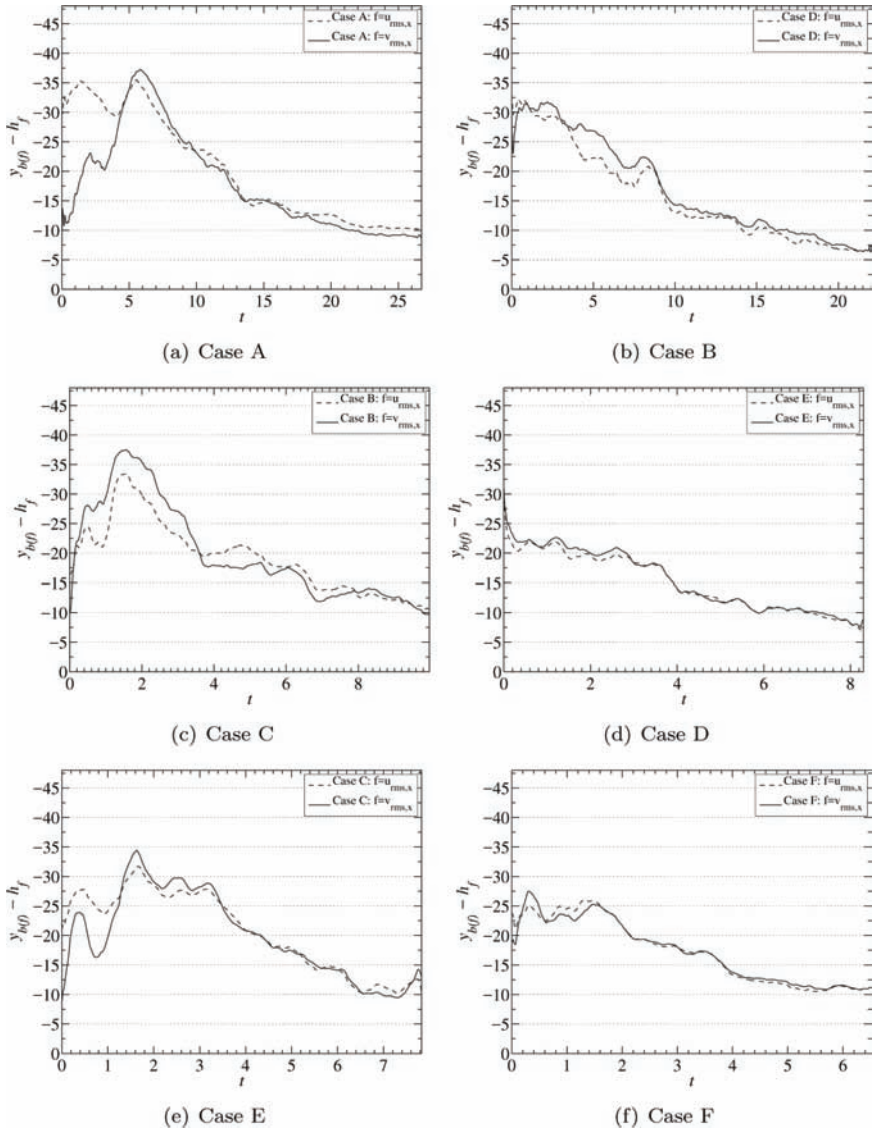

Figure 12. The plots show the distance from the surface of the network at which the 85% of E_f is confined for all cases. The solid line (–) shows the case where $f = v_{rms,x}$, instead (– –) corresponds to $f = u_{rms,x}$. Each line is obtained from the average of 3 realizations.

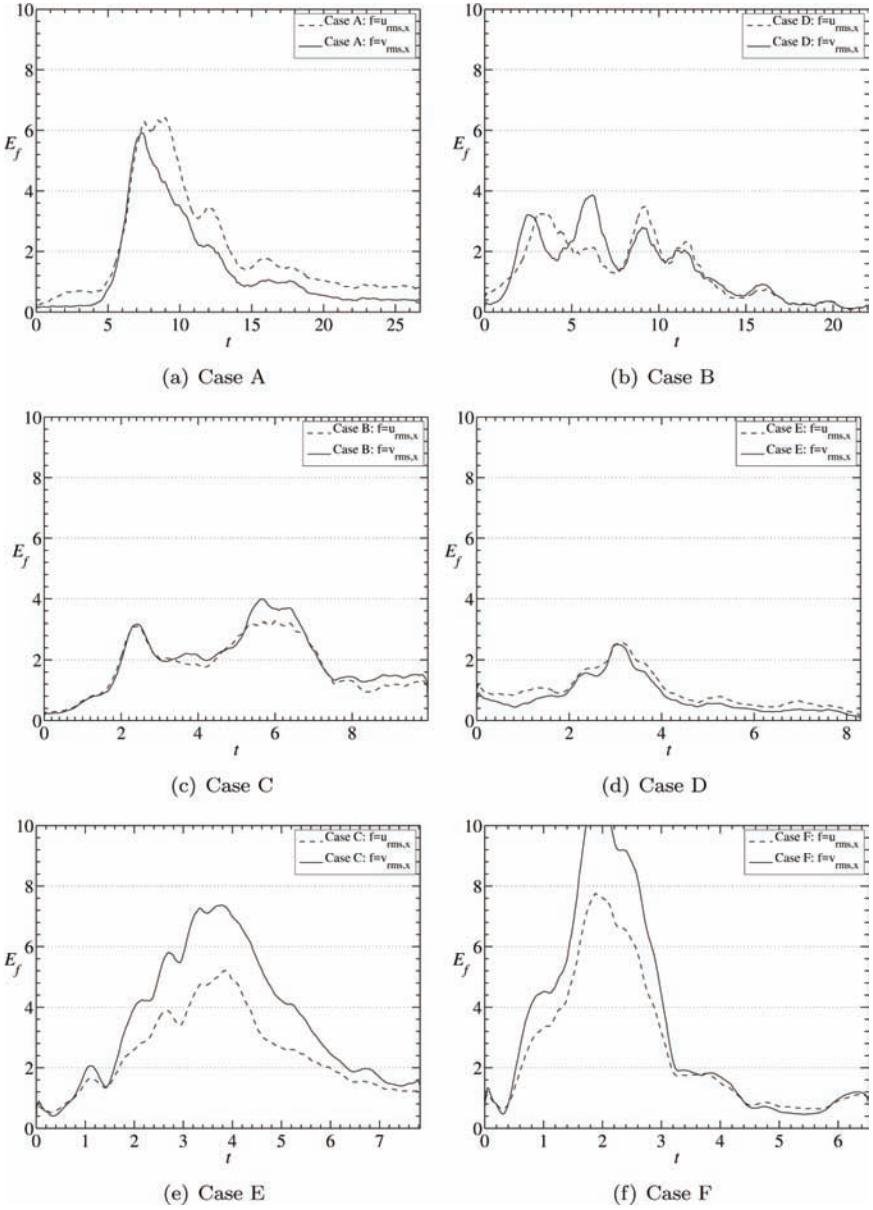

Figure 13. Time evolution of E_f for all experimental cases. The solid line (–) shows the case where $f = v_{rms,x}$, instead (– –) corresponds to $f = u_{rms,x}$. Each line is obtained from the average of 3 realizations.

4.5 Flow through the fiber network

Measurements inside the network are not easy to perform due to the presence of air bubbles and impurities between the camera and the region under study, and due to the complex geometry of the cavities formed in the fiber network. Therefore, the resulting data are noisy. Nevertheless, analysis of the data after the formation of the fibre network gives important insights on the flow through the cavities and of the structure and evolution of the network itself.

To measure the flow through the fiber network we apply the filtering procedure described in section 2.3. We then use PIV to measure flow velocity. Figure 14(a) show an instantaneous image of tracer particles flowing through the formed network, while 14(b) is the average over 400 instantaneous snapshots, showing the streamlines through the fiber network for Case F. It is clear that, while in the case of the flow through the forming wire (fig. 4) the streamlines where straight and regularly spaced, here they are much more irregular, since have to adjust to the inner structure of the network.

This can be seen observing the time evolution of the velocity from the PIV data. Figure 15(a) and (b) show the vertical velocity component v as a function of x and time at three different heights, y =?19, –12 *and* –10 for Case B and Case F. Here v has been normalized at each time step, to highlight the magnitude of velocity variations. The low velocity regions, are most likely areas occupied by fibers whereas, high velocity regions are cavities where the measured velocity is higher, thus this gives us the idea of the cavity size distribution inside the fiber network. At time $t = 0$ the flow is steady as the fibers did not start to pile up on the screen, and the flow is uniform in the cross-stream direction. Then large scale variation start to appear as the first fibers are deposited on the wire and after clear high and low velocity regions are formed according to the network structure. These length scales can be analyzed both in space and in time. Generally, after the

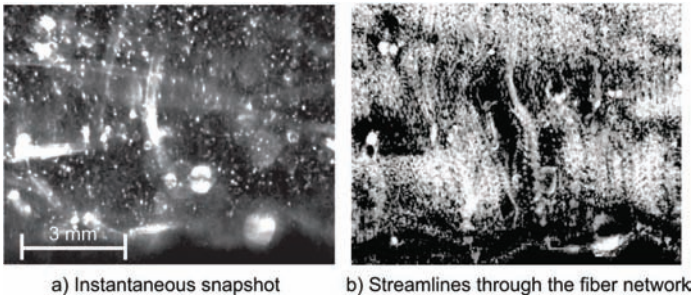

Figure 14. Streamlines through fiber network

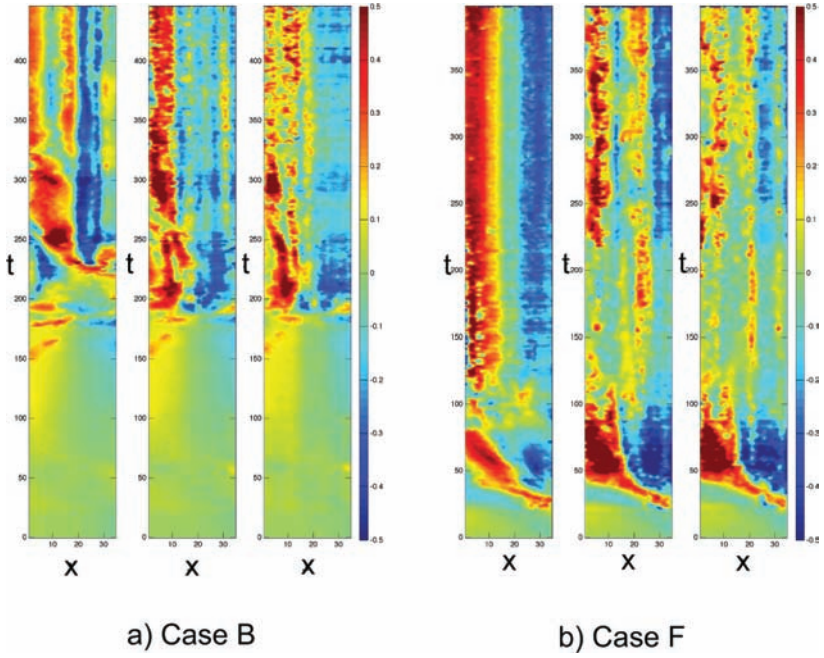

Figure 15. Instantaneous vertical velocity v as a function of horizontal position x and time t. In order to highlight the structures, the data is normalized at each time-step; y=–22 (*left*), y=–18 (*centre*) and y=–11 (*right*) for (a) Case B and (b) Case F.

network starts to form, these length scales decrease as time elapses. This might indicate that the fiber network is becoming more compact.

No large differences can be observed between the two cases shown here (both formed with short fibers), showing that filtration velocity, in the range tested here, has no big impact on the fiber network structure.

Although these are mainly qualitative indication of the flow through the network, it shows the potential of this technique to investigate flow and particle transport through a fibrous network, which is really important to predict filter efficiency and retention capability of a fibrous filter. It gives also an idea on the magnitude of the velocity variations occurring in the filter medium, which is important to determine the most appropriate flow models to be used in analytical studies and numerical simulations.

5 DISCUSSION AND CONCLUSIONS

Alaboratory apparatus designed to study the filtration of a fiber suspension in a parameter range close to that of the real papermaking process has been presented, together with an experimental procedure that combines index-of-refracion matching, high-speed imaging, and Particle Image Velocimetry (PIV) used to measure flow and particle dynamics.

Time resolved velocity measurements above and in a forming fiber network have been performed.

Three type of experiments are reported. The first two, without any fibers, are aimed at characterizing the flow in the test section in the near-wall region (i), and in the proximity of the screen (ii). For (i), the time evolution of the velocity profiles is investigated. A region not affected by the boundary layer was found for all the investigated cases. In that region, the flow was found to be stationary and homogeneous.

In (ii), experiments at three Reynolds number were conducted and it was concluded that the perturbations introduced by the screen are confined in a thin region (*boundary region*) close to the screen. The extension of the boundary region is independent of the Reynolds number based on the wire diameter of the screen and is about $2d_s$.

In the third type of experiments fibers were introduced in the flow. We performed six experimental cases with different combinations of filtration velocity and fiber aspect ratio. The results showed that the flow becomes time dependent and large and small scales fluctuations can occur.

For the case with the empty screen, the flow was found to be stationary, but when fibers have been included in the suspension, the flow during the filtration became time dependent.

The time dependency is introduced by the forming fiber network on top of the screen (time dependent boundaries), by the inherent instability of the free sedimentation of the fibers [12], and by the coupling between the two phenomena.

Velocity fluctuations are important because they are connected to the transport of material inside the domain (large scales), or to the change of orientation distribution (small scales).

In particular, from the measured boundary region y_b and strain rate ε, we can calculate the parameter $T_r = y_b/(V_m T)$, where T is the period for a fiber to perform one Jeffery's orbit [8]. T_r relates the residence time of a particle in the boundary region to the time required to perform a complete Jeffery's orbit. Thus it is a measure of how much the orientation distribution can change in the boundary region. The calculations show that $T_r < 0.05$ for all the cases, if y_b is taken from the measurements above the empty mesh. Therefore no significant variation of the orientation distribution can take place in this phase. This is also in agreement with

qualitative visual inspections of the flow images. For the cases with fibers instead, the estimation of T_r is not possible since the instantaneous velocity gradients are not available. However, it is reasonable to assume that due to the increase of y_b, also T_r increases slightly.

It has to be pointed out that T_r does not say anything about the change in mass distribution, which can still occur in this region. In fact, more fibers should be transported towards the areas of higher mass flow (corresponding to the location of the gaps).

Measurements of the flow in the fiber network showed the potential to: reveal the inner structure of the fiber network, analyze the magnitude of the velocity fluctuations inside the porous media and study particle transport through a fibrous network, which is really important to predict filter efficiency and retention capability of a fibrous filter.

Furthermore, the experiment presented here can also serve as a reference database for validation and development of numerical simulations.

5.1 Relevance for papermaking

Although this is a laboratory experiment where factors like jet-wire speed difference, fillers etc., are neglected, some of the observations are relevant for the industrial process of paper formations.

Even if the physical scales of the experiment are ten times larger than those of the papermaking, the governing parameters like the Reynolds number is of the same order in experiments and the real process (a detailed comparison can be found in [3]).

From the analysis of the flow above the mesh, which is important to determine the orientation of the first fiber layer, we observed that the dewatering velocity is less relevant since the position of the boundary region does not depend on the Reynolds number and is proportional to the gap size. Moreover, we have seen that in that region T_r is too small for relevant change in fiber orientation to occur. The network structure is thus defined by the incoming suspension and the direct contact between the wire and the fibers. However, when the network has begun to form, and the first fiber flocs has deposited on the screen, the size of the boundary region increases and scales with the floc size (thus approximately with the fiber length), hence, changes in fiber orientation due to the flow might be relevant.

The boundary region is also the region of non uniform dewatering velocity, which is responsible for the self-healing effect [9].

Finally, the capability shown here to measure the flow inside the fiber network can be used to study filler motion and accumulation during forming. The physics of this process is unknown to a large extent also on an empirical level. Insights would have a direct impact on the control and design of the product properties.

REFERENCES

1. S. Adanur. Effects of forming fabric structural parameters on sheet properties. *Tappi J*, **77**(10):187–195, Jan 1994.
2. M. Agelinchaab, M. F Tachie and D. W. Ruth. Velocity measurement of flow through a model three-dimensional porous medium. *Physics of Fluids*, **18**:017105, Jan 2006.
3. G. Bellani. 'Velocity Measurements in a Fiber Suspension Flow: Formation of a Fiber Network.' Licentiate Thesis, Royal Institute of Technology, Stockholm, 2008.
4. K. Chung, M. Simmons and M. Barigou. *A New piv Approach to Measuring Gas and Liquid Phase Velocities in a miniature stirred vessel*. 6th International Conference on Multiphase Flow, ICMF 2007, Leipzig, Germany, July 9–13, 2007, p. 11, June 2007.
5. P. Hampson. Fibre length and fabric aperture. *Proceedings from 52th Appita Annual Conference*, pp. 377–382, 1998.
6. Juergen Hoferer, Martin J. Lehmann, Edme H. Hardy, Joerg Meyer and Gerhard Kasper. Highly resolved determination of structure and particle deposition in fibrous filters by MRI. *Chem Eng Technol*, **29**(7):816–819, Jan 2006.
7. C. Holmqvist. 'Mechanical Modelling of Blade Forming and Drainage of Occulated Suspensions.' PhD Thesis, Royal Institute of Technology, Stockholm, Jan 2005.
8. G Jeffery. The motion of ellipsoidal particles immersed in a viscous fluid. *Proceedings of the Royal Society of London*. Series A, Jan 1922.
9. M. Lucisano and B. Norman. The forming and properties of quasi-random laboratory paper sheets. *Proceedings of International Paper Physics Conference, San Diego*, p. 11, July 2004.
10. F. Lundell, L. D. Söderberg and P. H.Alfredsson. Fluid mechanics of papermaking. *Annual Review of Fluid Mechanics*, **43**:195–217, Jan 2010.
11. A. Mark, E. Svenning, R. Rundqvist, F. Edelvik, E. Glatt, S. Rief, A. Wiegman, M. Fredlund, R. Lai, L. Martinsson and U. Nyman. Microstructure simulation of early paper forming using immersed boundary methods. *Tappi J*, **10**(11):7–14, Sep 2011.
12. B. Metzger, E. Guazzelli and J. E. Butler. Large-scale streamers in the sedimentation of a dilute fiber suspension. *Phys. Rev. Lett.*, **95**(16):164506–1–4, Jan 2005.
13. Uichiro Narusawa, J. T. Blucher and D. Goldthwaite. Analysis of melt infiltration into a moving bundle of fibers relevant to processing of metal matrix composite wires. *Journal of Porous Media*, **4**(3):1–10, Jan 2001.
14. M. Nordlund, S. Fernberg, and T. Lundström. Particle deposition mechanisms during processing of advanced composite materials. *Composites Part A*, **38**:2182–2193, Jan 2007.
15. C. Petrie. The rheology of fibre suspensions. *Journal of Non-Newtonian Fluid Mechanics*, **87**:369–402, Jan 1999.
16. R. Herzig and D. B. Johnson. Investigation of thin fiber mats formed at high velocity. *Tappi J*, Jan 1999.
17. Jeffrey A. Roux and Anil L. Jeswani. Impact of pull speed on wetout for a detached injection chamber in resin injection pultrusion. *Journal of Porous Media*, **13**(1): 13–27, Jan 2010.

18. M. R. Shahnazari and A. Vahabikashi. Permeability prediction of porous media with variable porosity by investigation of stokflow over multiparticles. *Journal of Porous Media*, Jan 2011.
19. M. Shams, I. G. Currie and D F. James. The flow field near the edge of a model porous medium. *Experiments in Fluids*, **35**:193–198, Jan 2003.
20. A. Tornberg and K. Gustavsson. A numerical method for simulations of rigid fiber suspensions. *Journal of Computational Physics*, **215**(1):172–196, June 2006.
21. Rahul Vallabh, Joel Ducoste, Abdel-Fattah Seyam and Pamela Banks-Lee. Modeling tortuosity in thin fibrous porous media using computational fluid dynamics. *Journal of Porous Media,* **14**(9):791–804, Jan 2011.
22. J. Westerweel. Fundamentals of digital particle image velocimetry. *Measurement Science and Technology*, **8**:1379–1392, Jan 1997.
23. P. Xiang, A. V. Kuznetsov and A.. Seyam. A porous medium model of the hydro entanglement process. *Journal of Porous Media*, **11**(1):35–49, Jan 2008.

Transcription of Discussion

EXPERIMENTAL STUDY OF FILTRATION OF FIBRE SUSPENSION

PART I

Gabriele Bellani,[1] *Fredrik Lundell*[1] *and L. Daniel Söderberg*[1,2]

PART II

Gabriele Bellani,[1] *Roland Bach,*[1] *Fredrik Lundell*[1] *and L. Daniel Söderberg*[1,2]

[1] Linné Flow Centre, KTH Mechanics, SE-100 44 Stockholm, Sweden
[2] Innventia AB, SE-114 86 Stockholm, Sweden

Kit Dodson University of Manchester, Mathematics

It was very nice to see those pictures. We worked on related things with much more primitive methods and it was brought to Oxford in 1965. The paper was called *The Detection and Cause of Layering in Paper*. At that time, we did not have the extremely good laser sheet light. We scratched the paint off the side of a transistor. It made it light sensitive and we had effectively a cafetière. For what this did was demonstrate that the fibres formed in a layered way and the additional part of the paper showed how to calculate the degree of layering. I don't see it mentioned, but it does say more or less what you have done, but using wood fibres.

Fredrik Lundell KTH Mechanics

Thank you very much. I can say that I am happy, that I am an experimentalist nowadays and not back then. The studies you did with the equipment you had is just amazing.

Discussion

Jean-Claude Roux Grenoble Institute of Technology

I would like to thank you for this very interesting presentation and I was very pleased to see your curve in the second case: Formation of a fibre network where you put the thickness of the fibrous network versus the fibre grammage. For both cases of speed and velocity 18.8mm/s and 64.6mm/s you get more or less the same slope. You probably know that in many modellings of the forming process on paper machines, we may assume that the fibrous mat, to a certain extent, has a solid consistency which is constant: whatever the increase of the pressure drop. On your pictures, you get this result which is very interesting because for the first time it's not an hypothesis, but a fact.

Fredrik Lundell

Thank you. In this context I would like to emphasize that this is filtration from a 0.5% suspension. If one is interested in thickening, there is a bit more work to do.

Joel Panek WestRock

I am not familiar with this area and the images and the graphics look fascinating. What is the biggest contribution of this work to the advances in our research? What do you think is the one or two things that we should take away from this work?

Fredrik Lundell

I think the big thing is probably the experiment as such. With this, we could also look at filler transported in the fibre mat. If we could find good ways to manipulate the adhesion between these fibres and some scaled filler particles, we could look at filler transport through the fibre web with different agglomerates etc. So, I think that if there is anything that is a long-term contribution to the field, except for things that were only hypothesized on, then it's the fact that we have an experiment where we can look at such things in a consistent manner.

Joel Panek

Okay. I guess the development of experimental techniques is directly observed.

Fredrik Lundell

Yes. Also, there is a community working with cut fishing line as model fibres and in that community our fibre ends are quite good.